Electronic Supplementary Material (ESI) for Journal of Materials Chemistry A.

Electronic Supplementary Information

Interfacial electron-engineered tungsten oxynitride interconnected rhodium layer for highly efficient all-pH-value hydrogen production

Ben Zhang,[#] Yijuan Zheng,[#] Zhenyu Xing, Zihe Wu, Chong Cheng, Tian Ma,* and Shuang Li*

#These authors contributed equally to this paper.

Country College of Polymer Science and Engineering, State Key Laboratory of Polymer Materials Engineering, Sichuan University, Chengdu 610065, China

Electronic supplementary Information to DOII: http://doi.org/10.1039/

Experimental Section

1. Materials and Chemicals

Table S1 Experimental materials and chemicals

Chemicals	Concentration	Company
Tungsten(VI) chloride (WCl_6)	99%	Aladdin
Rhodium(III) chloride hydrate ($RhCl_3·xH_2O$)	98%	Aladdin
Urea	99.5%	Aladdin
potassium hydroxide (KOH)	85%	Aladdin
Ethanol (C_2H_5OH)	99.7%	Aladdin
Platinum on carbon (Pt/C)	20%	Alfa Aesar
Nafion D520	5 wt%	Alfa Aesar
Rhodium on carbon (Rh/C)	10%	Energy Chemical
Ketjenblack	99.9%	Canrd

All chemicals were from commercial sources and used without further purification. Ultrapure water was used for the preparation of all aqueous solutions.

2. Synthesis of Rh-WNO

200 mg of WCl6 and 10 mg of $RhCl_3•xH_2O$ powder were dispersed in ethanol (2 ml) to form a stable and transparent solution. Add 200 mg of urea to the above solution and stir to dissolve. Then 20 mg of Ketjen black (KB) was added, stirred for 30 min, and then transferred to a crucible for aging and complexation for 12 h to obtain a gel-like solid. The above operations are done in the glove box. The gel was placed in a tube furnace in an Ar gas environment (flow rate 100 mL min^{-1}), and the temperature was raised to 70 °C at a heating rate of 1 °C/min and kept at a constant temperature for 2 h. After that, the temperature continued to rise to 600 °C at a heating rate of 5 °C/min and held at a constant temperature for 3 h. Cool to room temperature and passivate for 2 hours under the same argon flow. The obtained product was ground for use. Initial slow heating is important to avoid burst release of residual solvent. At a high temperature of 200 °C, urea is decomposed into NH_2, NH_3, HNCO, and H_2NCO groups to participate in the nitridation reaction. To analyze the effect of pyrolysis temperature on HER performance, the solid powders were pyrolyzed at 500, 700, 800, and 900 °C for 3 h. (Denoted as: Rh-W-500, Rh-W-700, Rh-W-800 and Rh-W-900) The preparation process of WNO is the same as that of Rh-WNO, except that $RhCl_3•xH_2O$ is not added to the solution.

Table SS1.

Samples	$RhCl_3·xH_2O$	WCl_6	urea	Temperature
Rh10mg-WNO	10 mg	200 mg	200 mg	600 °C
Rh5mg-WNO	5 mg	200 mg	200 mg	600 °C
Rh20mg-WNO	20 mg	200 mg	200 mg	600 °C
Rh-W-500	10 mg	200 mg	200 mg	500 °C
Rh-W-700	10 mg	200 mg	200 mg	700 °C
Rh-W-800	10 mg	200 mg	200 mg	800 °C
Rh-W-900	10 mg	200 mg	200 mg	900 °C
WNO		200 mg	200 mg	600 °C
Rh-WO_3	10 mg	200 mg		600 °C
Rh-KB	10 mg		200 mg	600 °C

3. Characterization

3.1 Scanning electron microscopy (SEM)

SEM images were obtained by using a Thermo Fisher Scientific (FEI) Apreo S HiVoc. The gold coating was deposited with a layer of about 1 nm.

3.2 Aberration-corrected high-angle annular darkfield scanning transmission electron microscope (AC HAADF-STEM)

AC HAADF-STEM was performed on a JEOL JEM-ARM 200F scanning transmission electron microscope equipped with a cold field emission electron source and a DCOR probe corrector (CEOS GmbH), a 100 mm2 JEOL Centurio EDX detector, and a Gatan GIF Quantum ERS electron energy-loss spectrometer) operated at 200 kV.

3.3 X-ray diffraction (XRD)

Powder XRD of all the prepared samples was measured by Rigaku Ultima IV with Cu Kα irradiation.

3.4 X-ray photoelectron spectra (XPS)

XPS measurements were performed on K-Alpha™+ X-ray Photoelectron Spectrometer System (Thermo Scientific) with Hemispheric

180° dual-focus analyzer with 128-channel detector and a monochromatic Al Kα irradiation.

3.5 X-ray absorption spectra (XAS)

XAS spectra were collected on the beamline BL07A1 in NSRRC (National Center for Synchrotron Radiation Research). The radiation is by scanning a Si (111) double-crystal monochromator.

4. Electrochemical Measurements

Ink preparation: The catalyst ink was prepared by blending the catalyst powder (W-based materials: 15 mg; materials without W: 10 mg) with 100 µL Nafion solution (5 wt. %) and 900 µL ethanol in an ultrasonic bath. 5 µL of catalyst ink was then pipetted onto the GC surface (0.196 cm^2). The TOF data was calculated based on the atomic content (from XPS) of the Rh or Pt in the catalysts.

Electrodes and measurements: All the electrochemical measurements were carried out in a conventional three-electrode cell using the Gamry reference 600 workstations (Gamry, USA) at room temperature. A commercial RHE electrode was used as the reference electrode, and the graphite rod was used as the counter electrode. The Ag/AgCl reference electrode calibrated with RHE in 1 M KOH was used as a reference electrode for long-term stability measurement. A glassy carbon (GC) RDE electrode with an area of 0.196 cm2 served as the substrate for the working electrode to evaluate the HER activities of various catalysts. The electrochemical experiments were conducted in Ar-saturated 1 M KOH, 0.5 M H_2SO_4, and 1 M PBS electrolyte. The polarization curves of different catalysts with real-time iR were corrected by Gamry reference 600 potentiostats at a resistance of 4.4 ohms. The RDE measurements were conducted at a rotating speed of 1600 rpm with a sweep rate of 10 mV/s. The stability tests for the catalysts were conducted using chronopotentiometry at the constant working current densities of 10 mA/cm2.

The electrochemically active surface area was estimated by measuring the capacitance of the double layer at the solid-liquid interface with cyclic voltammetry. The measurement was performed in a potential window of 0.88–0.98 V versus RHE, where the Faradic current on the working electrode was negligible. The series of scan rates ranging from 50 to 300 mV s^{-1} was applied to build a plot of the charging current density differences against the scan rate at a fixed potential of 0.93 V. The slope of the obtained linear curve was twice the double-layer capacitance (C_{dl}).

The TOF values were calculated as the number of oxygen molecules evolved per active site per second based on the following equation:

$$TOF = \frac{J * A}{4F * m}$$

Where J is the current density (A cm^{-2}), A is the effective surface geometric area of the working electrode (0.196 cm^{-2}), F is the Faraday constant, and n is the number of active metals on the electrode. The TOF data was calculated based on the weight content (from XPS) of the noble metals (Pt or Rh) in the catalysts.

Supplementary Images:

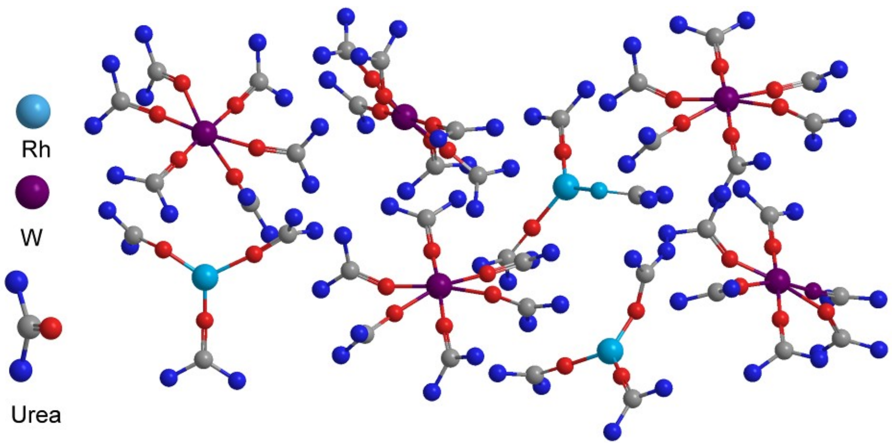

Figure S1. Schematic illustration of the metal-urea precursor.

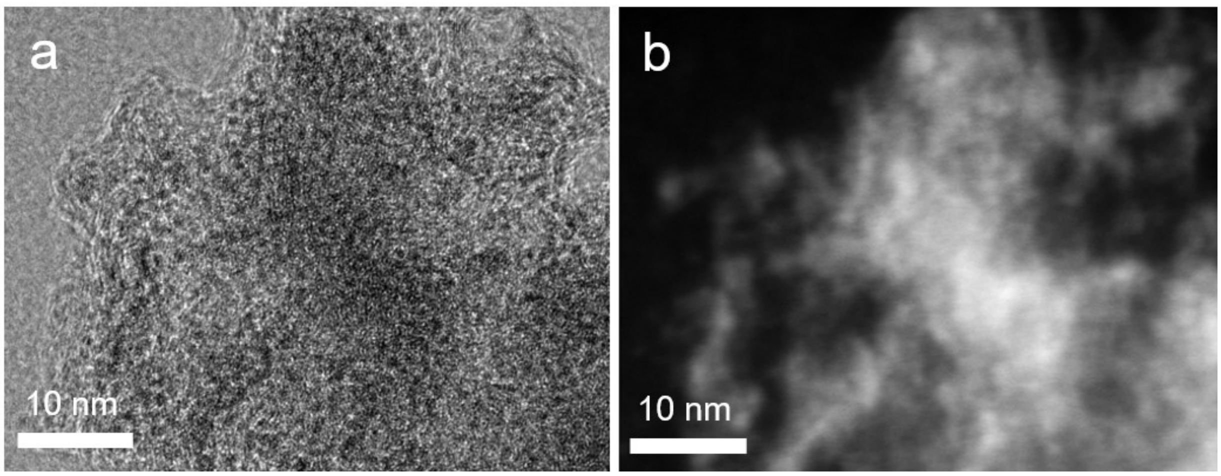

Figure S2. a) Bright-field TEM image of Rh-WNO; b) dark-field TEM image of Rh-WNO.

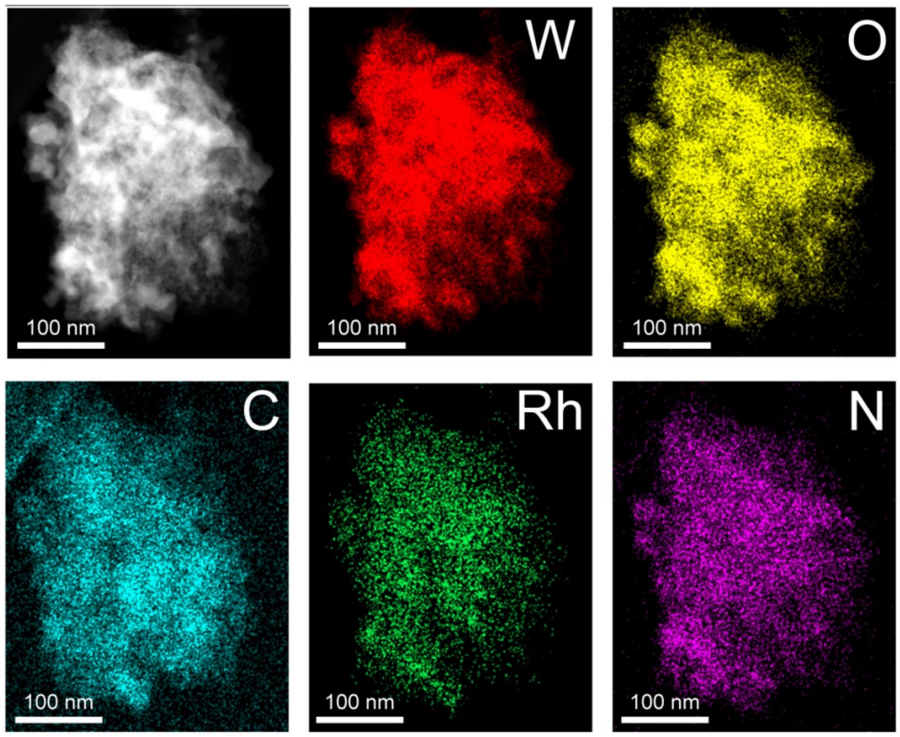

Figure S3. EDX mapping of Rh-WNO.

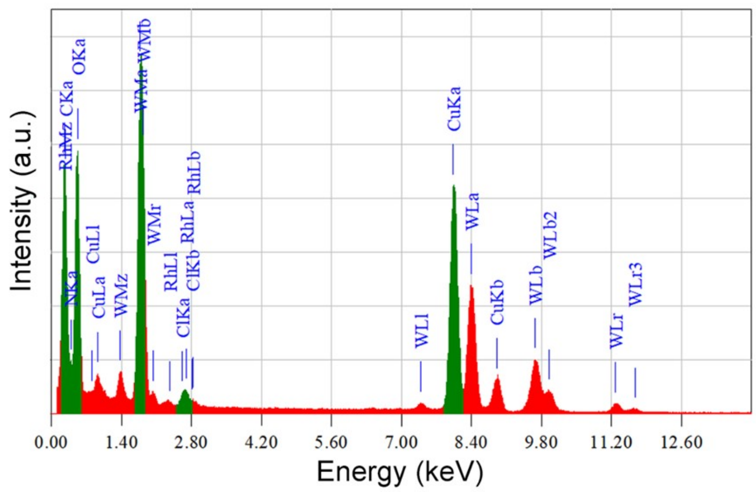

Figure S4. EDX pattern of Rh-WNO.

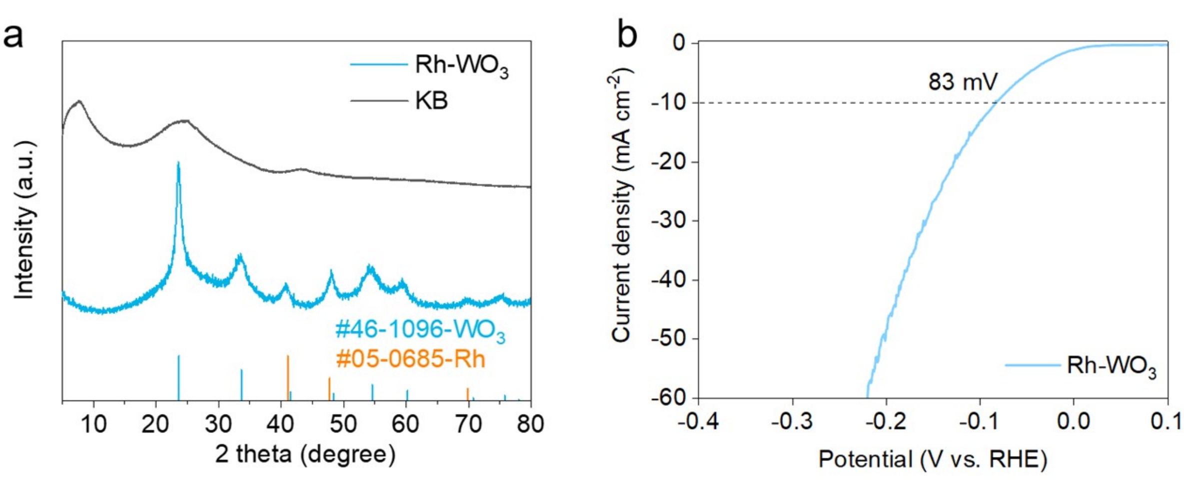

Figure S5. a) XRD spectra of KB and Rh-WO_3. b) LSV curves of Rh-WO_3 in 1.0 M KOH.

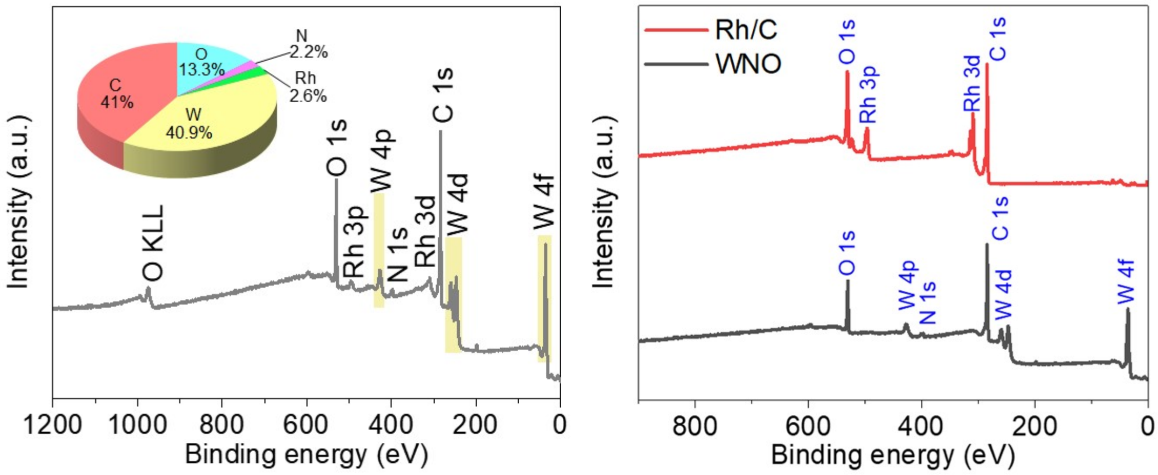

Figure S6. XPS survey scans of Rh-WNO, WNO, and Rh/C.

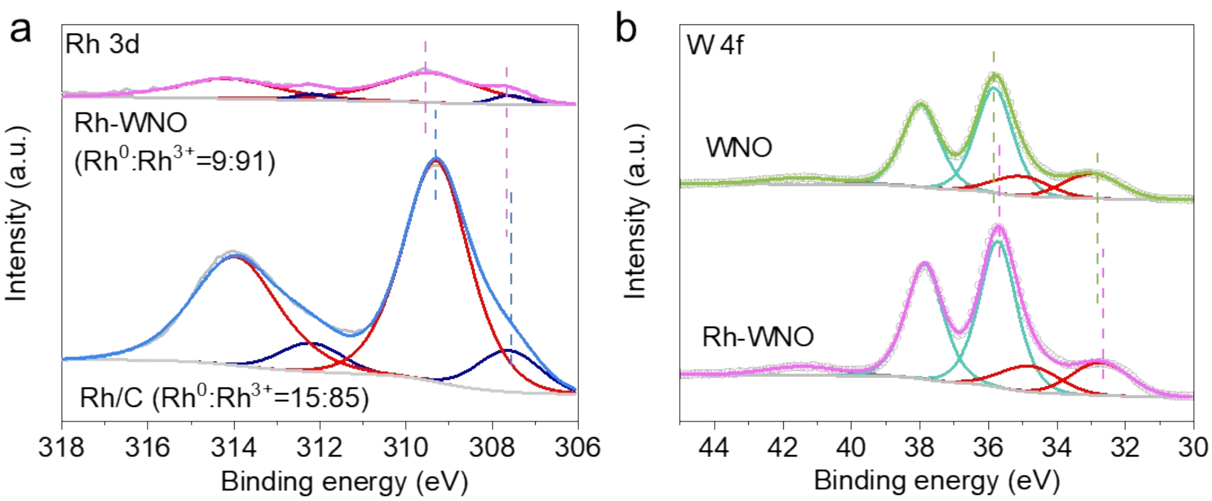

Figure S7. (a) XPS spectra of Rh 3d for Rh-WNO and Rh/C. (b) XPS spectra of W 4f for Rh-WNO and WNO.

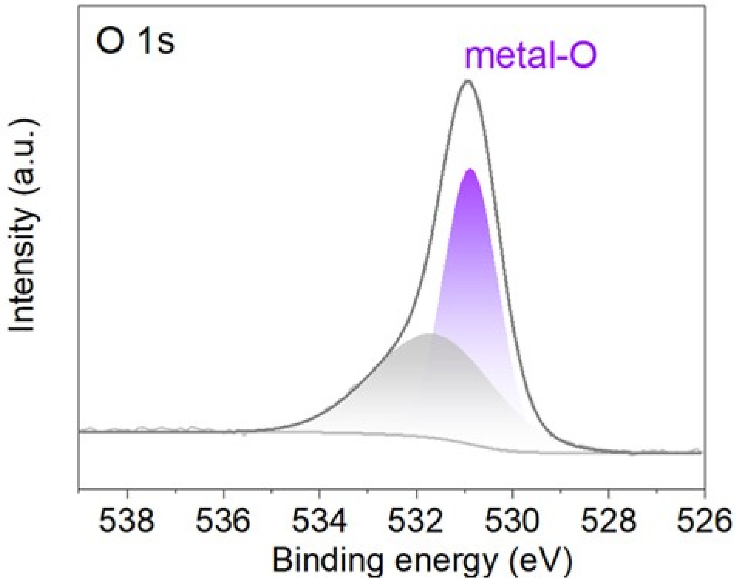

Figure S8. XPS spectra of O 1s for Rh-WNO.

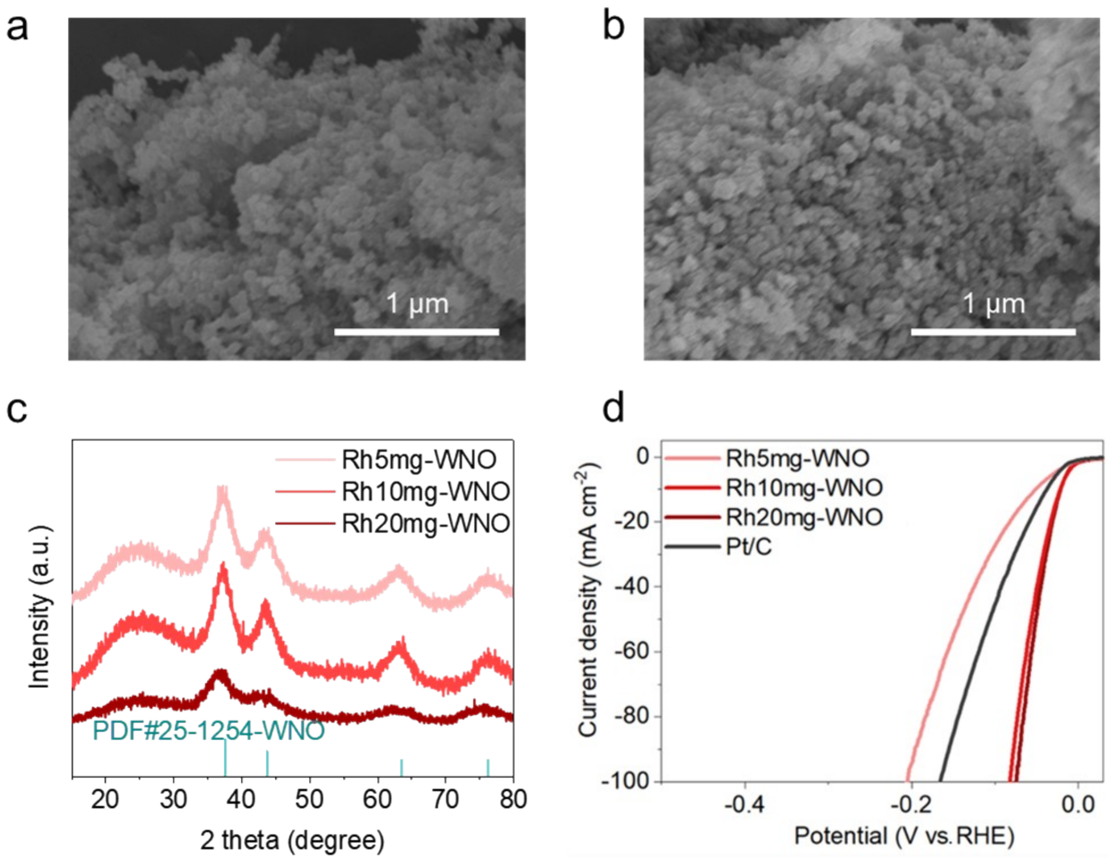

Figure S9. SEM images of a) Rh5mg-WNO, and b) Rh20mg-WNO. c) XRD patterns, and d) LSV curves of Rh-WNO with different Rh feeding in 1.0 M KOH.

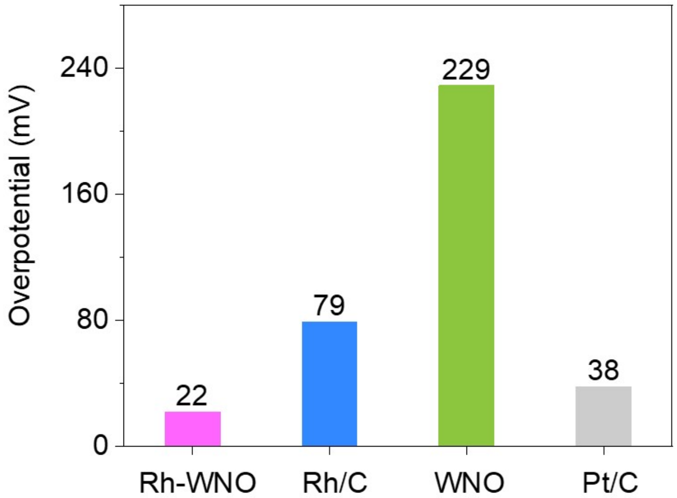

Figure S10. Comparison of the overpotentials at 10 mA cm^{-2}.

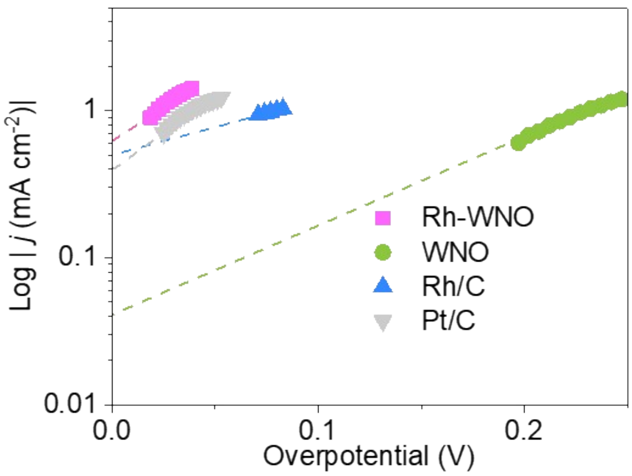

Figure S11. Exchange current densities for different catalysts.

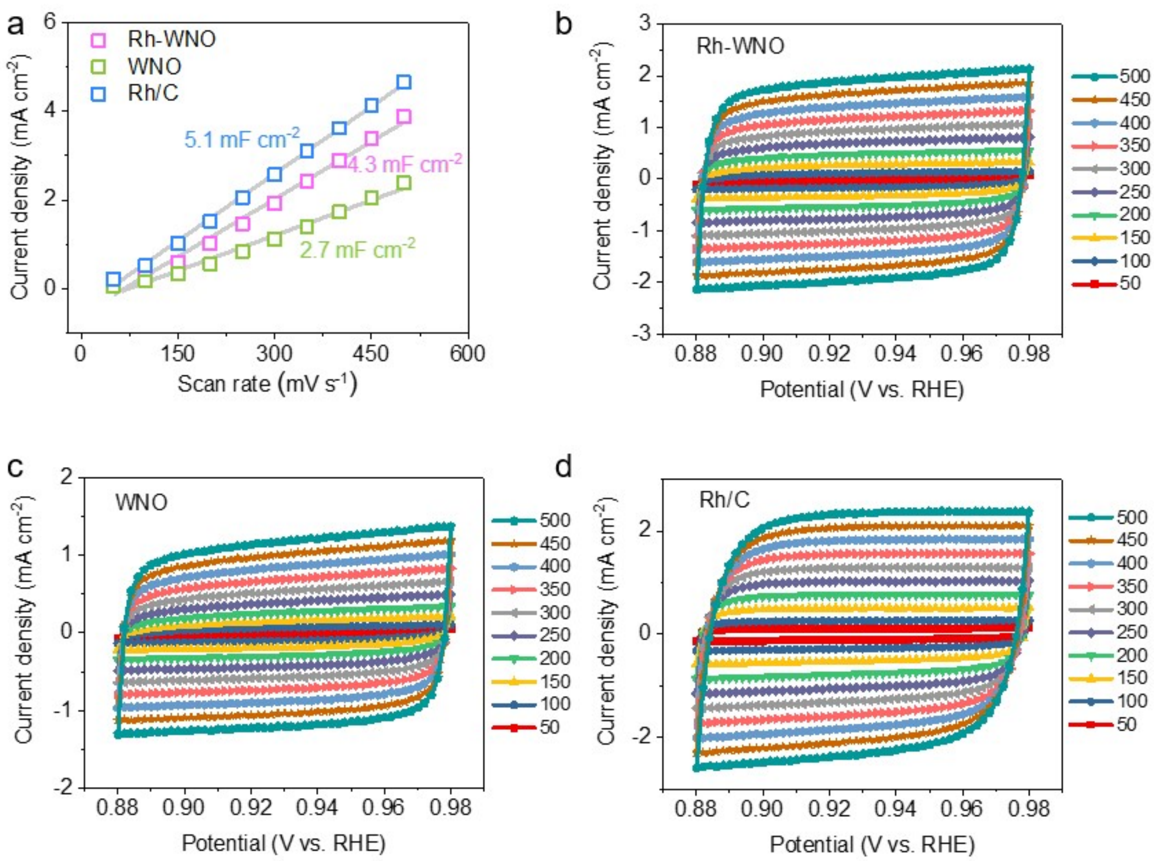

Figure S12. (a) C_{dl} plots inferred from CV curves. Cyclic voltammograms of (b) Rh-WNO, (c) WNO, and (d) Rh/C in 1 M KOH at different scan rates in the non-Faradaic potential region (0.88-0.98 V versus RHE).

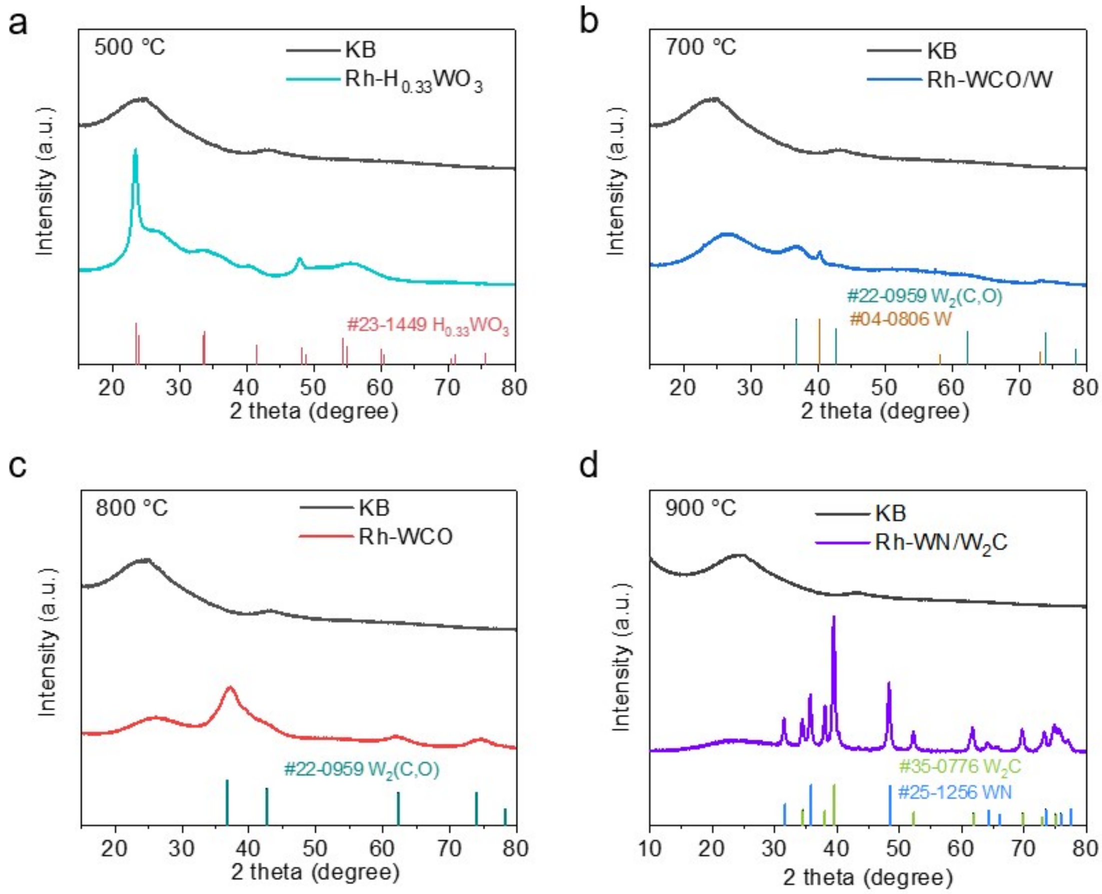

Figure S13. The XRD patterns of Rh-WNO prepared at (a) Rh-$H_{0.33}WO_3$ at 500 °C, (b) Rh-WCO/W at 700 °C, (c) Rh-WCO at 800 °C, and (d) Rh-WN/W_2C at 900 °C.

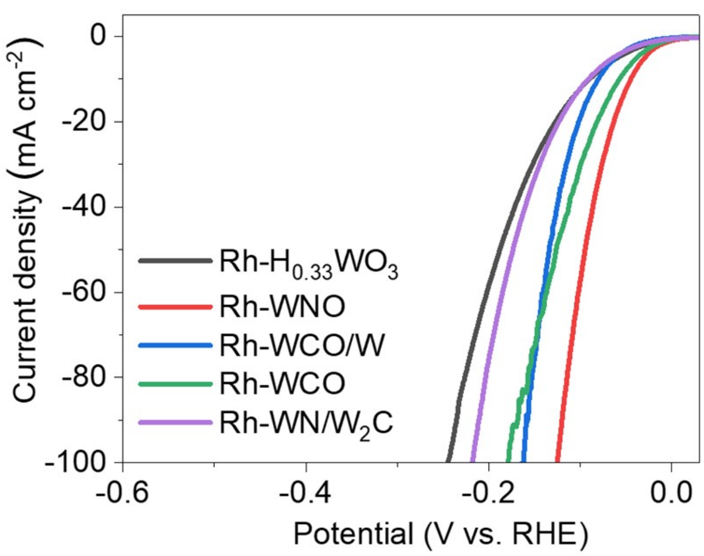

Figure S14. LSV curves of Rh-$H_{0.33}WO_3$, Rh-WNO, Rh-WCO/W, Rh-WCO, and Rh-WN/W_2C.

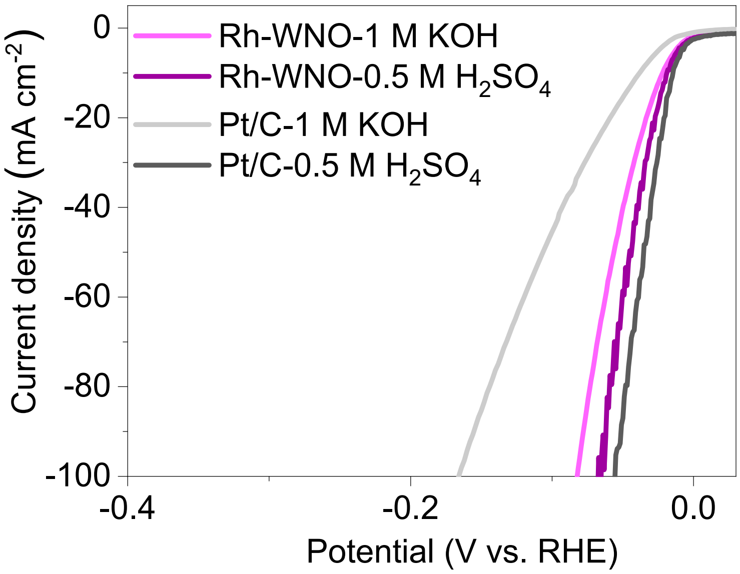

Figure S15. HER polarization curves of Rh-WNO and Pt/C in 1 M KOH and 0.5 M H_2SO_4.

Table S2 Comparison of HER activities of Rh-WNO with reported catalysts

Catalysts	Overpotential at 10 mA cm^{-2} (mV)	Tafel slope (mV dec^{-1})	Noble metal Content (%)	MA at −100 mV (A mg^{-1})	TOF at −100 mV(s^{-1})	Reference
Rh-WNO	22	34.7	2.58	5.47	7.84	This work
Rh-MoS_2	47	24	5.20	13.87, η=250 mV	-	1
Rh_2P	30	50	58.1	-	-	2
Rh-$MoSe_2$	73	123	8.20	-	-	3
Rh_6Cu_1 NPs	36	35	85.8	-	-	4
Rh SAC-CuO NAs/CF	44	-	6.80	-	-	5
Ru-NiCo-LDH	28	42	16.4	-	-	6
Pt_{SA}-$Co(OH)_2$	39	35.7	2.80	1.6 A mg^{-1}	-	7
Rh-doped CoFe-ZLDH	28	42.8	20.00	-	-	8
Rh–Rh_3Se_4/C	29	110.6	5.00	1.97, η=50 mV	1.06, η=50 mV	9
Rh-CoNi LDH/MXene	74.6	43.9	6.00	-	-	10
Rh NP@BNS	101	47	5.00	-	-	11
Rh/N-CBs	77	74.16	4.50	-	-	12

Table S3 The atomic weight ratio on the sample surface determined by XPS.

Samples		C	N	O	Rh	W
Rh-WNO	wt.%	40.97	2.23	13.30	2.58	40.92
	at.%	72.13	3.93	17.33	0.53	6.07

References

1. Y. Cheng, S. Lu, F. Liao, L. Liu, Y. Li and M. Shao, *Advanced Functional Materials*, 2017, **27**.
2. F. Yang, Y. Zhao, Y. Du, Y. Chen, G. Cheng, S. Chen and W. Luo, *Advanced Energy Materials*, 2018, **8**.
3. Y. Zhao, C. Yang, G. Mao, J. Su, G. Cheng and W. Luo, *Inorganic Chemistry Frontiers*, 2018, **5**, 2978-2984.
4. W. Zhang, J. Zhao, J. Zhang, X. Chen, X. Zhang and F. Yang, *Acs Applied Materials & Interfaces*, 2020, **12**, 10299-10306.
5. H. Xu, T. Liu, S. Bai, L. Li, Y. Zhu, J. Wang, S. Yang, Y. Li, Q. Shao and X. Huang, *Nano Letters*, 2020, **20**, 5482-5489.
6. D. Li, B. Zhang, Y. Li, R. Chen, S. Hu and H. Ni, *Electrochemistry Communications*, 2019, **101**, 23-27.
7. K. L. Zhou, C. Wang, Z. Wang, C. B. Han, Q. Zhang, X. Ke, J. Liu and H. Wang, *Energy & Environmental Science*, 2020, **13**, 3082-3092.
8. K. Zhu, J. Chen, W. Wang, J. Liao, J. Dong, M. O. L. Chee, N. Wang, P. Dong, P. M. Ajayan, S. Gao, J. Shen and M. Ye, *Advanced Functional Materials*, 2020, **30**.
9. S. Pan, S. Ma, C. Chang, X. Long, K. Qu and Z. Yang, *Materials Today Physics*, 2021, **18**.
10. L. Yan, D. Song, J. Liang, X. Li, H. Li and Q. Liu, *Journal Of Colloid And Interface Science*, 2023, **640**, 338-347.
11. K. Chen, Z. Wang, L. Wang, X. Wu, B. Hu, Z. Liu and M. Wu, *Nano-Micro Letters*, 2021, **13**.
12. N. Jia, Y. Liu, L. Wang, P. Chen, X. Chen, Z. An and Y. Chen, *Acs Applied Materials & Interfaces*, 2019, **11**, 35039-35049.